Insulin Allosteric Behavior: Detection, Identification, and Quantification of Allosteric States via ^{19}F NMR†

Maria Bonaccio,§ Nima Ghaderi,‡ Dan Borchardt,‡ and Michael F. Dunn*,§

Departments of Biochemistry and Chemistry, University of California at Riverside, Riverside, California 92521

Received March 1, 2005; Revised Manuscript Received April 11, 2005

ABSTRACT: The insulin hexamer is an allosteric protein widely used in formulations for the treatment of diabetes. The hexamer exhibits positive and negative cooperativity and apparent half-site binding activity, reflecting the interconversion of three allosteric states, designated as T_6, T_3R_3, and R_6. The hexamer contains two symmetry-related Zn^{2+} located 16 Å apart on the 3-fold symmetry axis. In the transition of T_3 units to R_3 units, Zn^{2+} switches from an octahedral $Zn^{2+}N_3O_3$ complex (N is HisB10, O is H_2O) to a distorted tetrahedral $Zn^{2+}N_3L$ complex (L is a monovalent anion). Hence, monovalent anions are allosteric ligands that stabilize R_3 units of T_3R_3 and R_6. Herein, we exploit the high sensitivity of ^{19}F NMR chemical shifts and fluorinated carboxylates to reveal subtle differences in the anion-binding sites of T_3R_3 and R_6. We show that the chemical shifts of 4- and 3-trifluoromethylbenzoate and 4- and 2-trifluoromethylcinnamate give bound resonances that distinguish between T_3R_3 and R_6. 3-Trifluoromethylbenzoate and 2-trifluoromethylcinnamate also were shown to bind to the R_3 units of T_3R_3 and R_6 in two alternative, slowly interconverting modes with different microenvironments for the CF_3 groups. Line width analysis shows that ligand off rates are slower by $1/10^3$ than the diffusion limit, indicating a rate-limiting protein conformational transition. These studies confirm that the Seydoux, Malhotra, and Bernhard allosteric model (Bloom, C. R., Choi, W. E., Brzovic, P. S., Ha, J. J., Huang, S. T., Kaarsholm, N. C., and Dunn, M. F. (1995). *J. Mol. Biol. 245*, 324−330), provides a robust description of the insulin hexamer.

The allosteric properties of the zinc insulin hexamer strongly influence the stability and dynamic properties of insulin (*1*, *2*), and likely play critically important roles in the synthesis, assembly, and storage of insulin in the β-cells of the pancreas (*3*−*5*). The allosteric behavior of the insulin hexamer has become an important paradigm for allosteric behavior; the hexamer exhibits positive and negative[1] homotropic and heterotropic interactions and half-site reactivity (*6*−*13*). The binding of allosteric ligands to the insulin hexamer also plays an important role in the design of insulin formulations for use in the treatment of diabetes.

Three global conformation states[2] of the insulin hexamer have been identified by crystallographic analysis. These have been designated as T_6, T_3R_3, and R_6[3] (*6*). The conformational transition from a T_3 unit of the hexamer to an R_3 unit involves the conversion of residues 1−9 of the insulin B-chain from an extended conformation to α-helix (*14*−*16*). This transformation gives a 3-helix bundle aligned along the hexamer 3-fold symmetry axis that creates an amphipathic site involving the HisB10 zinc ion and forms hydrophobic pockets located at the interfaces between R-state subunits. Consequently, interconversion between these three allosteric forms is modulated by the binding of phenol and derivatives of phenol to the hydrophobic pockets (the phenolic pockets) of the R-state hexamers (three in T_3R_3 and six in R_6) and by the binding of monovalent anions, including halides, pseudohalides, and organic carboxylates coordinated to the HisB10 sites (one in T_3R_3 and two in R_6) (*1*, *6*, *7*, *9*, *17*). The phenolic pockets are located at the interfaces between the subunits of the R_3 units of T_3R_3 and R_6. The HisB10 anion sites are located on the 3-fold symmetry axes of T_3R_3 and R_6. The phenolic pockets within an R_3 unit are ∼20 Å distant from each other; the two zinc sites within a hexamer are ∼ 16 Å distant, and the closest distance between a phenolic pocket and a HisB10 site is approximately 6−8 Å.

In the absence of allosteric ligands, the insulin hexamer exists predominantly in the T_6 state. The T_3R_3 state can be

† Supported by a gift from Novo Nordisk to M.F.D.

* Corresponding author. Phone: 951-827-4235. Fax: 951-827-3719. E-mail: michael.dunn@ucr.edu.

‡ Department of Chemistry, University of California at Riverside.

§ Department of Biochemistry, University of California at Riverside.

[1] The designation, "negative cooperativity", is used empirically to denote binding isotherms exhibiting shapes consistent either with apparent affinities which become weaker as ligand concentration is increased or to denote binding isotherms which appear to saturate at a site occupancy less than the total number of sites (i.e., half-site reactivity).

[2] The terminology, "global conformational state", is used here and throughout to designate the folding (i.e., secondary and ternary structural elements) of insulin subunits within the hexamer. For the purposes of this discussion, localized perturbations of the folded structure arising from weak bonding interactions between ligand and protein are not considered here to be separate global conformation states.

[3] Abbreviations: T_6, T_3R_3, and R_6, the global conformations of insulin hexamer forms with extended (T) and α-helical (R) conformations of B-chain residues 1−9; SMB, half-site reactivity (sub-optimal symmetry) model for cooperativity; L_0^A and L_0^B, the allosteric constants for the interconversions of T_6 with T_3R_3 and T_3R_3 with R_6, respectively; K_R and K_R^0, the dissociation constants for binding to the phenolic pockets of R_6 and T_3R_3, respectively; ρ, the fraction of R-state species, ^{19}F NMR, fluorine nuclear magnetic resonance; 4TFMB and 3TFMB, 4- and 3-trifluoromethylbenzoate, respectively; 4TFMC and 2TFMC, 4- and 2-trifluoromethylcinnamate, respectively.

10.1021/bi050392s CCC: $30.25
Published on Web 05/07/2005

stabilized by the binding of thiocyanate ion (*6*, *17*, *18*) or certain phenolic ligands (*10*−*12*, *19*), and the R_6 state is stabilized by the binding of the combination of phenolic ligands and monovalent anions (*1*, *9*, *14*, *17*). The T_6 and R_6 species possess one 3-fold and three pseudo-2-fold axes of symmetry. The pseudo-2-fold axes of symmetry have their origins in a slight asymmetry in the dimeric units of T_6 and R_6 (*4*, *14*, *20*). Because of the large difference in B-chain conformations within a TR dimeric unit, the T_3R_3 species retains only a 3-fold symmetry axis and no pseudo-2-fold-symmetry axes.

Our previous studies have extensively documented the allosteric behavior of the insulin hexamer and its importance in the design of insulin formulations for treatment of diabetics (*1*, *2*, *6*, *9*, *11*, *12*, *17*, *21*). The work of Bloom et al. (*11*−*13*) has demonstrated that the Seydoux, Malhotra, and Bernhard model (the SMB model) (*22*) for mixed positive and negative cooperativity and half-site reactivity in ligand binding provides a subunit-based symmetry/asymmetry model that unites both the crystallographic structural data and the solution allosteric behavior into a detailed mechanistic hypothesis for the allosteric behavior of the insulin hexamer. We have postulated that when appropriately tailored to the insulin hexamer, the SMB model provides a quantitative description of the allosteric behavior that relates the symmetry properties of the T_6, T_3R_3, and R_6 conformation states to the positive and negative cooperativity and half-site reactivity of the hexamer (*12*). Encouraged by the success of the SMB model in quantifying the allosteric behavior of the hexamer, we have undertaken additional studies to further test the applicability of the model. To accomplish this, we have developed a new set of ligands for the HisB10 anion site that incorporate ^{19}F NMR probes which allow us to identify and characterize the hexamer conformation states present in solution under conditions where there is a net interconversion between the T- and R-states driven by the binding of phenolic ligands. These studies establish that trifluoromethyl-substituted benzoates and cinnamates are sensitive probes of insulin conformation in solution and are capable of distinguishing between the T_3R_3 and R_6 states of the Zn(II)- and Co(II)-substituted insulin hexamers. As will be shown, this sensitivity to conformation state in the insulin system arises from the following factors: (1) the sensitivity of ^{19}F chemical shifts to small changes in environment is relatively high (for example in comparison to ^{1}H chemical shifts) (*23*−*27*), (2) the formation of bound states that are in slow exchange with the free ligand on the NMR time scale, and (3) the simplicity of the ^{19}F NMR spectra of complexes obtained with ligands containing CF_3-substituents. As will be shown in this study, we have succeeded for the first time in detecting and quantifying the number and distribution of allosteric conformation states present in the T- to R-state transitions of the insulin hexamer.

In comparison to the monomer, hexameric forms of insulin are very stable to denaturation and chemical degradation. The equilibria among T_6, T_3R_3, and R_6 are modulated by the binding of allosteric ligands to the phenolic pockets and to the HisB10 sites. We previously have shown that the mass action effects of the binding of allosteric ligands can render the R_6 state more stable than the T_3R_3 or T_6 states by 2−6 orders of magnitude (*2*). Therefore, molecules with improved characteristics that stabilize the T_3R_3 and R_6 states are potential stabilizing agents for use in insulin pharmaceutical formulations for the treatment of diabetes. The unusual 3-fold symmetry of the HisB10 anion site makes this site an interesting subject for ligand design. Huang et al. (*29*) showed that aromatic carboxylates comprise a new class of very promising HisB10 ligands. The information obtained in this study offers important new insights of potential relevance to the design of allosteric effectors for use as stabilizing agents in insulin formulations.

MATERIALS AND METHODS

Materials. Metal-free human insulin was a gift supplied by Novo Nordisk (Denmark). The chemicals employed in these studies were reagent grade or better and were used without further purification. Zinc sulfate was purchased from Mallinckrodt. Cobalt perchlorate was purchased from Alpha products. D_2O was purchased from CIL, Inc. All other reagents were purchased from Sigma Aldrich.

Instrumentation. UV/visible absorbance spectra were collected using a Hewlett-Packard 8452A spectrophotometer.

^{19}F NMR spectra were collected on a Varian Inova 500 MHz NMR spectrometer, equipped with a 5 mm Nalorac ^{1}H/^{19}F probe operating at a frequency of 470.56 MHz. Data were accumulated as 16 384 complex point FIDs at 25 °C with a relaxation delay of 2 s over a spectral width of 28 429 Hz (56 ppm). A total of 256 transients were accumulated and averaged for each experiment. Spectra were processed with 3 Hz line broadening apodization applied. Reported ^{19}F chemical shifts (δ) are referenced against an external trifluoroacetic acid standard ($\delta = 0.00$ ppm).

Experimental Procedures. Insulin monomer was dissolved in 50 mM Tris/$HClO_4$, pH 8.0, buffer, and concentration was determined by UV/visible absorbance, using the extinction coefficient $\epsilon_{280} = 5700\ M^{-1}cm^{-1}$ (insulin monomeric unit). $Co(ClO_4)_2$ and $ZnSO_4$ stock solutions were prepared in double deionized water and not in buffer to avoid formation of hydroxides at pH 8.0. The concentrations of Zn^{2+} and Co^{2+} were determined by absorbance titration using the chromophoric chelator, terpy (*2*, *28*). Insulin hexamers were prepared by adding the metal ion solutions into the insulin monomer solution in a molar ratio of 2:6.

Phenol, 2,7-DHN, and carboxylates were dissolved in 50 mM Tris/$HClO_4$, pH 8.0, buffer, and pH was corrected to 8.0 with 2.5 M KOH. When ligand solubility was too low, ethanol was added as a cosolvent in a maximum concentration of 20% v/v.

^{19}F NMR samples were prepared in aqueous buffers containing 10% D_2O (v/v) and locked on the D_2O field frequency. No pH correction was made for the D_2O content. Metal-site ligand binding curves measured by ^{19}F NMR or UV/vis absorbance spectroscopy were performed under the following conditions: [insulin hexamer] = 1 mM, [phenol] = 100 mM, D_2O 10% (v/v) in 50 mM Tris, pH 8.0, at 25 °C. Phenol and 2,7-DHN titrations by ^{19}F NMR were conducted for both Zn(II)- and Co(II)-substituted insulin hexamers in the following conditions: [insulin hexamer] = 1 mM and [carboxylate] = 10 times the value of K_{Dapp}, D_2O 10% (v/v) in 50 mM Tris, pH 8.0, at 25 °C.

Titrations of Co(II)-substituted insulin hexamer with phenol and 2,7-DHN were also followed by UV/vis spectrophotometry using the same conditions reported above.

Scheme 1: SMB Allosteric Model for the Positive and Negative Cooperativity and Half-Site Reactivity of the Insulin Hexamer[a]

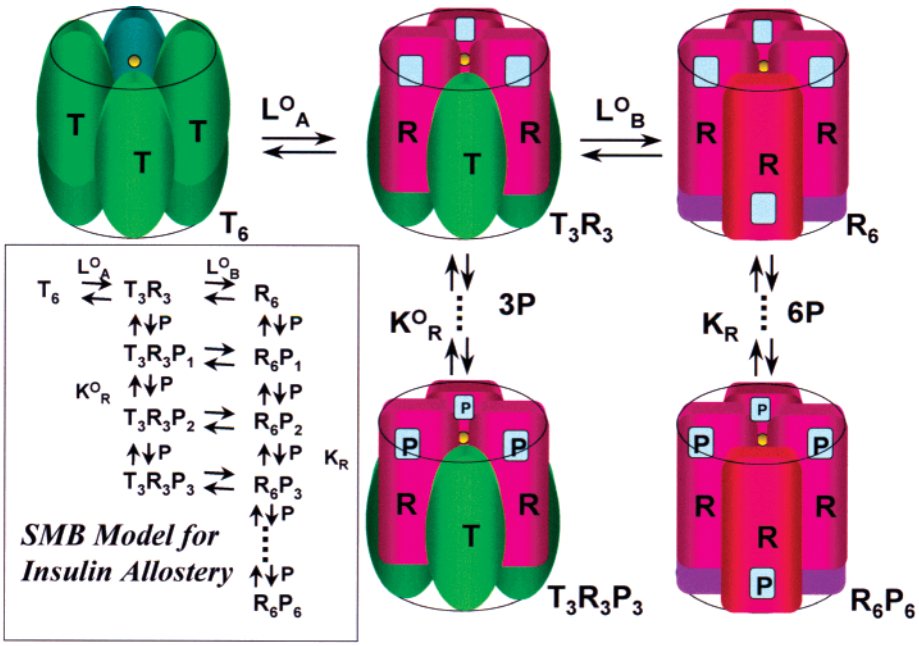

[a] Insulin subunits are designated as T-state (light and dark green ellipsoidal solids) and R-state (light and dark magenta rectangular solids), and the hexamer conformation states are identified as T_6, T_3R_3, or R_6. The HisB10 metal ions are shown as gold balls; the phenolic pockets are shown as small white rectangles. The allosteric constants, L_0^A and L_0^B, describe the interconversion of T_6 and T_3R_3 and the interconversion of T_3R_3 and R_6, respectively. The inset shows the detailed set of equilibria for the binding of a phenolic ligand, P, with dissociation constants K^0_R and K_R for the T_3R_3 and R_6 states, respectively.

The ligands investigated were 2-trifluoromethylcinnamate (2TFMC), 4-trifluoromethylcinnamate (4TFMC), 3-trifluoromethylbenzoate (3TFMB), and 4-trifluoromethylbenzoate (4TFMB).

Apparent dissociation constant (K_{Dapp}) values were calculated for the R_6 state of the cobalt hexamer by following the spectral changes in the Co(II) d−d transitions resulting from the displacement of phenolate by fluorocarboxylates from the HisB10 site (*29*). Ligand binding curves to the cobalt hexamer were fit using eq 1 (*29*):

$$\Phi = \Phi_{max}\,[L]_f/(K_{Dapp} + [L]_f) \qquad (1)$$

where Φ is the relative absorbance, with $0 < \Phi < 1$; Φ_{max} is the highest relative absorbance value; $[L]_f$ is the free ligand concentration, $[L]_{free} = [L]_{tot} - [L]_{bound}$. K_{Dapp} is the apparent dissociation constant of the ligand for the protein. UV/vis titration curves for the binding of phenol and 2,7-DHN to the Co(II)-substituted insulin hexamer were fitted using the SMB model (Scheme 1, eq 2) (*10*),

$$\rho = [(0.5L_0{}^B(1+\beta)^3) + (1+\alpha)^6]/ [(L_0{}^B(1+\beta)^3) + (1+\alpha)^6 + L_0{}^A L_0{}^B] \qquad (2)$$

Where ρ is the fraction of sites in the R state; $L_0{}^A = [T_6]/[T_3R_3]$; $L_0{}^B = [T_3R_3]/[R_6]$; α = [phenolic ligand]/K_R; and β = [phenolic ligand]/K^0_R. For phenol titrations, α and β were locked to the published values (*11*), and the allosteric constants $L_0{}^A$ and $L_0{}^B$ were calculated.

^{19}F NMR peaks corresponding to the bound ligand species were fit using a Lorentzian (eq 3) or a sum of two, three, or four Lorentzian equations. For a single Lorentzian,

$$y = a_0/[\pi a_2 + (1 + (x - a_1/a_2)^2)] \qquad (3)$$

where a_0 is the peak area, a_1 is the peak chemical shift, and a_2 is the peak width. The fitted peak areas were plotted versus phenol or 2,7-DHN concentration. Titration curves for the total bound species with phenol or 2,7-DHN were fitted to the SMB model (Scheme 1) using eq 2. For titrations of the Co(II)−insulin hexamer, the allosteric constants $L_0{}^A$ and $L_0{}^B$ were calculated from the UV/vis titration, and these values were locked in the fitting of the ^{19}F NMR titrations. To calculate allosteric constants from titrations of the Zn(II)-substituted insulin hexamer, the values for K_R and $K_R{}^0$ calculated previously were locked in for the fitting analysis. Equation 2 accounts for the contribution to the saturation by sites of both the T_3R_3 and R_6 conformations according to the SMB model. Modifications of eq 2 quantify the contribution from T_3R_3 only (eq 4) or from R_6 only (eq 5)

$$\rho_{T3R3} = [0.5L_0{}^B(1+\beta)^3]/ [(L_0{}^B(1+\beta)^3) + (1+\alpha)^6 + L_0{}^A L_0{}^B] \qquad (4)$$

$$\rho_{R6} = (1+\alpha)^6/[(L_0{}^B(1+\beta)^3) + (1+\alpha)^6 + L_0{}^A L_0{}^B] \qquad (5)$$

RESULTS

Binding of Trifluoromethyl-Substituted Aromatic Carboxylates to the HisB10 Sites of the Insulin Hexamer. The d-d transitions of Co(II)-substituted insulin hexamer are strongly altered by the change in coordination geometry that accompanies the conversion of the pseudotetrahedral R_6 phenolate complex to the 5-coordinate R_6 carboxylate complex (*17*, *29*, *30*). The apparent dissociation constants

Table 1: Summary of Apparent and Specific Dissociation Constants for the Binding of Trifluoromethyl-Substituted Aromatic Carboxylates to the Zn(II)- and Co(II)-Substituted Insulin Hexamers

HisB10 ligand	K_{Dapp} (mM)		K_D (mM)[b]	
	zinc[a]	cobalt	zinc	cobalt
3TFMB	0.16	0.28 ± 0.027	0.014	0.025
4TFMB	0.88	1.59 ± 0.014	0.078	0.14
2TFMC	0.28	0.51 ± 0.02	0.025	0.045
4TFMC	0.92	1.65 ± 0.08	0.081	0.15

[a] Huang et al. (*29*) showed that the ratio $^{Co}K_{Dapp}/^{Zn}K_{Dapp}$ of anionic ligands between zinc hexamer and cobalt hexamer is 1.8 for a wide range of ligand structures. Using this relationship, we estimated the K_{Dapp} values for the zinc hexamer. [b] The values of intrinsic K_D are calculated using eq 11, assuming a value for $K_{phenolate}$ of 9.7 mM.

for the binding of the trifluoromethyl-substituted aromatic carboxylates to the Co(II)-substituted insulin hexamer were determined using this spectral change and the methods developed by Huang et al. (*29*). These values are given in Table 1 for the trifluoromethyl-substituted aromatic carboxylates used in this study. According to Huang et al. (*29*), the Zn(II) complex has higher affinity for organic carboxylates than does the Co(II) complex by a factor of 1.8. Therefore, the K_{Dapp} values for the zinc hexamer (Table 1) were estimated by multiplying the corresponding values for the cobalt hexamer by the factor 1.8.

^{19}F NMR Studies of 3-Trifluoromethylbenzoate Binding to the Zinc Hexamer. Figure 1A shows 1D ^{19}F NMR spectra of the 3-trifluoromethylbenzoate (3TFMB) complex with the phenol-stabilized zinc insulin hexamer under experimental conditions where the concentration of 3TFMB is present in large excess of the protein sites. The ^{19}F NMR spectra show the presence of a single, sharp signal arising from the unbound species with a chemical shift of 15.49 ppm, and a broadened envelope of peaks corresponding to bound species with chemical shifts in the range of 16.9 to 17.0 ppm. The envelope of bound peaks appears to consist of four resonances and is well-described by the sum of four Lorentzians at every phenol concentration. In Figure 1B, an example of the fitting of the 3TFMB-bound peaks to the sum of four Lorentzian curves is shown. The presence of four distinct peaks (located respectively at 16.982, 16.949, 16.918, and 16.884 ppm) demonstrates that the ligand exchange processes between free and bound states and the exchange among bound states are slow compared to the NMR time scale. Spectra measured as a function of temperature (data not shown) established that the spectra of bound species are temperature-independent over the range of 5−35 °C. As the temperature was increased above 35 °C, the bound peaks gradually coalesced into a single, broad peak at about 70 °C. This behavior indicates that, at room temperature, both the exchange between free and bound states and the exchange among bound states are slow with respect to the ^{19}F NMR time scale.

The properties of both free and bound peaks (area, chemical shift, and line width) depend on the concentration of phenol (the ligand bound to the phenolic pocket). When increasing concentrations of phenol are added to the zinc insulin hexamer in the presence of 3TFMB, the amount of the bound species increases and then saturates as the conversion of T_6 to R_6 is completed. It is therefore possible to calculate the ratio of the concentration of bound 3TFMB

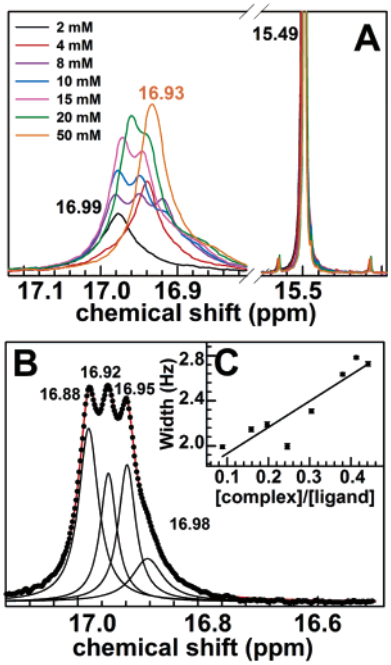

FIGURE 1: (A) 1D ^{19}F NMR spectra of 3TFMB in the presence of the zinc insulin hexamer and increasing phenol concentrations. The free peak has a chemical shift of 15.49 ppm (referenced to trifluoracetate ion). The bound species is an envelope of four peaks. (B) Example of the deconvolution of the envelope of bound 3TFMB peaks in the presence of the zinc insulin hexamer and 8 mM phenol, using the program Peakfit. The envelope of bound species (black dots) is fitted as four peaks (black Lorentzian curves) which sum to give the red curve (eq 2, Materials and Methods). (C) Dependence of the width of the 3TFMB free peak on the [complex]/[ligand] ratio. The width was calculated by fitting the free peak with a single Lorentzian equation at every 3TFMB concentration. The complex/ligand ratio was calculated both from the relative peaks areas and from eq 10.

to the concentration of free 3TFMB from the ratio of the areas of the bound and free peaks, respectively. If it is assumed that the binding of 3TFMB is a second-order exchange process and that the two HisB10 sites are kinetically equivalent and independent, then the binding equilibrium is given by eq 6

$$\text{Site} + 3\text{TFMB} \underset{k_{off}}{\overset{k_{on}}{=}} \text{Complex} \qquad (6)$$

where

$$K_D = k_{off}/k_{on} = [\text{Site}][3\text{TFMB}]/[\text{Complex}] \qquad (7)$$

It follows that the lifetime of the ligand in the unbound state is given by eq 8

$$\tau^{3TFMB} = \tau^{free} = 1/(k_{on}[\text{Site}]) = [3\text{TFMB}]/k_{off}[\text{Complex}] \qquad (8)$$

According to Lian and Roberts (*31*), the line widths of the resonances of the free ligand will be additive (eq 9)

$$1/T_2^{obs} = [(1/T_2^{free}) + (1/\tau^{free})] = \{(1/T_2^{free}) + (k_{off}[\text{Complex}]/[3\text{TFMB}])\} \qquad (9)$$

Consequently, k_{off} may be determined from a plot of the line width of the free ligand resonance versus the ratio [Complex]/[3TFMB]$_f$. The ratio [complex]/[ligand]$_f$ can be determined by calculating the ratio of the intensities of the bound peak and the free peak at every phenol concentration. In accord with the prediction of eq 9, the width of the free 3TFMB peak was found to increase linearly with the ratio [complex]/[3TFMB]$_f$ = [complex]/[ligand]. This approach gave a value for $k_{off} = 2.27\ s^{-1}$.

Alternatively, the [complex]/[ligand] ratio can be derived from the eq 7,

$$K_D = k_{off}/k_{on} = [\text{sites}][\text{ligand}]/[\text{complex}]$$

and

$$[\text{complex}]/[\text{ligand}] = [\text{sites}]/K_D \qquad (10)$$

The value of k_{off} obtained from this approach was $2.17\ s^{-1}$.

Similar results were obtained by titrating the phenol-stabilized insulin hexamer (R_6 state) with increasing concentrations of 3TFMB. When 0.25, 0.5, or 1.0 equiv of ligand is added to the zinc hexamer, the area, but not the chemical shift, of the bound peak changes. At concentrations of 3TFMB greater than the concentration of protein sites, the chemical shift of the free ligand did not change. This finding further indicates that the free ligand and the bound ligand are in slow exchange. When the free ligand is in excess, the free peak narrows. Again, as shown in Figure 1C, the width of the free peak increases linearly with the ratio [complex]/[ligand] (Figure 1C). The value of k_{off} obtained was $2.17\ s^{-1}$.

When increasing concentrations of 3TFMB are added to the phenol-stabilized zinc insulin hexamer (Figure 2A), the area under the envelope of bound peaks increases and then tends toward a saturated value. Figure 2A presents the dependence of the total area of the envelope of bound peaks versus the concentration of 3TFMB in the presence of phenol-stabilized zinc hexamer. The end-point for this titration curve (Figure 2A) is consistent with the formation of a complex exhibiting a stoichiometry of 2 mol of 3TFMB bound per mole of the phenol-stabilized zinc−insulin hexamer.

Figure 2B presents a plot of relative absorbance (defined as $\Phi = \Delta Abs/\Delta Abs_{Total}$ at $\lambda = 570$ nm) showing the dependence of the UV/vis absorption spectrum of the phenol-stabilized, cobalt-substituted insulin hexamer on the concentration of 3TFMB. This titration curve also is consistent with a stoichiometry of 2 mol of 3TFMB bound per mole of hexamer (given by the *x*-axis intercept at the vertical dashed line).

^{19}F NMR Studies of the Binding of 3- and 4-Trifluorimethylbenzoates to the 2,7-DHN-Stabilized Insulin Hexamer. To establish the degree of specificity with which 3TFMB binds to the HisB10 anion site of the R_3-unit of the T_3R_3 hexamer, experiments were conducted to determine if 3TFMB and SCN^- compete for the same site. The complex of 3TFMB with the 2,7-DHN-stabilized hexamer (a T_3R_3 species) (*10*, *11*) was titrated with increasing concentrations of SCN^- (Figure 2C,D). The ^{19}F NMR spectra shown in Figure 2C establish that SCN^- displaces 3TFMB. As the concentration of SCN^- increases, the peak corresponding to 3TFMB bound to the hexamer decreases in amplitude and then disappears. When the area of the bound peak was plotted versus the concentration of SCN^- (Figure 2D), the sharply descending limb of the resulting titration curve extrapolates to an intercept with the *x*-axis indicating an apparent stoichiometry of approximately 1.0:1.0 for the displacement of 3TFMB by SCN^-.

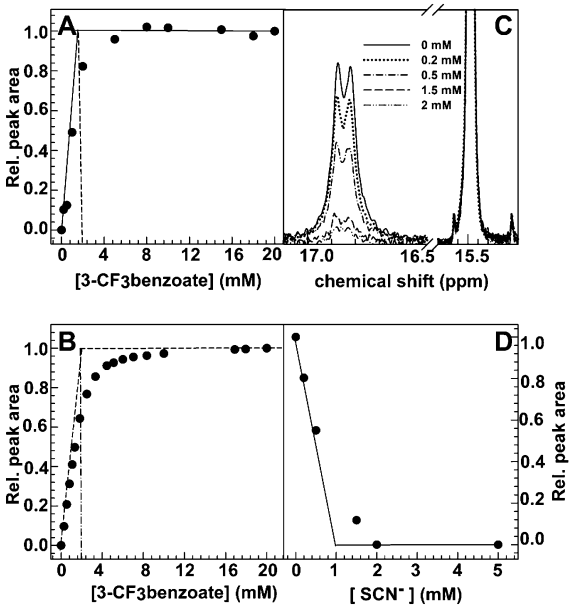

FIGURE 2: (A) Stoichiometry of 3TFMB binding to the R_6 zinc−insulin hexamer. Black dots represent the total area of ^{19}F NMR bound peaks. The *x*-intercept (dashed line) corresponds to a binding stoichiometry of 2.0 molecules of 3TFMB per hexamer. (B) Absorbance titration measured at 570 nm for the binding of 3TFMB to the R_6 cobalt−insulin hexamer. The *x*-intercept corresponds to a binding stoichiometry of 2.0 molecules of 3TFMB per hexamer, in good agreement with the ^{19}F NMR titration (A). (C) 1D ^{19}F NMR spectra showing the competition between 3TFMB and SCN^- for the 2,7-DHN-stabilized T_3R_3 zinc hexamer. The free peak of 3TFMB has a chemical shift of 15.49 ppm, while the bound species consists of an envelope of two peaks, with chemical shifts of 16.82 and 16.87 ppm, respectively. Upon addition of SCN^-, the areas of the bound peaks decrease and finally disappear. (D) Plot of relative area for the bound peaks shown in (C) versus the concentration of SCN^-. The titration endpoint (intersection of the straight lines) corresponds to a stoichiometry of one site per hexamer. Experimental conditions: zinc−insulin hexamer, 1 mM; 3TFMB, 6 mM; 2,7-DHN, 6 mM; D_2O 10% (v/v); 50 mM Tris buffer, pH 8.0, 25 °C.

When 4-trifluoromethylbenzoate (4TFMB) binds to the 2,7-DHN-stabilized form of the zinc insulin hexamer, the complex gives a 1D ^{19}F NMR spectrum (Figure 3A) consisting of a sharp peak located at 15.42 ppm, corresponding to the free ligand, and a broad envelope of one or more resonances in the 16.0−16.4 ppm region. It was found that this broad peak could be fitted with a single broad Lorentzian. However, at the highest 2,7-DHN concentrations, it appears that there are at least two peaks, one accounting for more than 80%, the remainder by the smaller peak. With the assumption that this envelope actually consists of two peaks, then this broad band was fitted with two Lorentzians (Figure 3B, solid dots and open squares). When the concentration of 4TFMB is held constant and in large excess over the zinc−insulin hexamer while the concentration of 2,7-DHN is varied (Figure 3A,B), chemical shifts and the line widths of the bound and the unbound peaks change. The areas of the bound peaks increase with increasing 2,7-DHN concentrations and

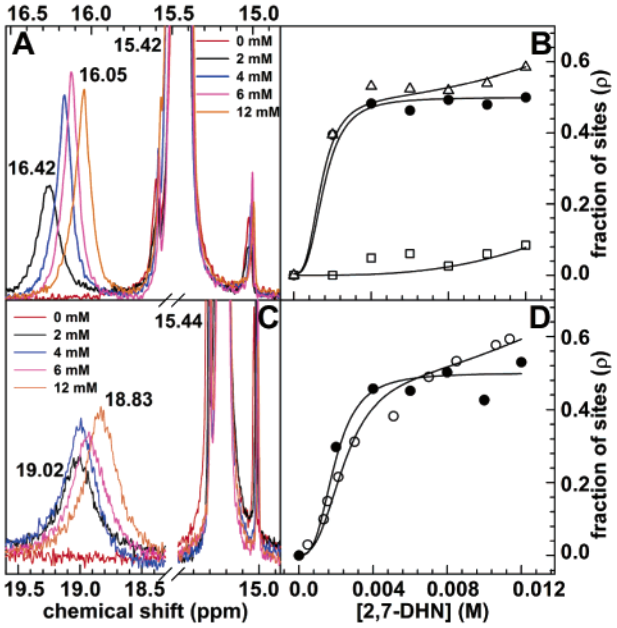

FIGURE 3: (A) 1D ^{19}F NMR spectra of 4TFMB in the presence of the zinc hexamer at different 2,7-DHN concentrations. The free peak of 4TFMB has a chemical shift of 15.42 ppm. The observed chemical shift of the 4TFMB-bound species depends on the 2,7-DHN concentration and varies from 16.42 ppm at 2 mM to 16.05 ppm at 12 mM. (B) ^{19}F NMR 2,7-DHN titration of the zinc hexamer in the presence of 4TFMB. The values of relative area for the bound peak are calculated by fitting the bound species as a combination of two Lorentzian equations. Assignments: solid circles represent T_3R_3, open squares represent R_6, and open triangles represent the total peak area. Solid lines represent the best fitting of ρ_{T3R3}, ρ_{R6}, and ρ for the T_3R_3, R_6, and R_{total} species for the SMB model (Scheme 1), respectively, as described by eqs 4, 5, and 2. (C) 1D ^{19}F NMR spectra of 4TFMB in the presence of the cobalt hexamer at different 2,7-DHN concentrations. The 4TFMB free peak has a chemical shift of 15.44 ppm, the bound peak depends on 2,7-DHN concentration and varies from 19.02 ppm at 2 mM to 18.83 ppm at 12 mM. (D) Comparison of the ^{19}F NMR and UV/visible titrations of the cobalt−insulin hexamer with 2,7-DHN in the presence of 4TFMB. Solid circles represent the total area of the ^{19}F NMR bound peaks; open circles represent the relative absorbance measured for the cobalt hexamer. Solid lines represent the best fitting of R-species formation (ρ) using eq 2.

then become concentration-independent; the line widths narrow, and the peak positions shift upfield (Figure 3A). The downfield peak (black dots) accounts for more than 80% of the total area of bound species. The upfield peak (open squares) increases to less than 10% of the total. Comparisons with Figure 2 show that the total area of these two peaks approaches a value that corresponds to a stoichiometry of one site per hexamer. The sum of these two peaks (open triangles) gives a saturation curve that is well-described by the SMB model (eq 2 in Materials and Methods), giving values of K_R and K_R^0 comparable to values calculated by Bloom et al. (*11*) for 2,7-DHN (Table 2). The curve for the predominating peak was well-fitted by the equation for the dependence of the T_3R_3 species (eq 4), while the minor peak was well-fitted by eq 5, which describes the dependence of the R_6 state upon the phenolic ligand concentration. Both the fitting of T_3R_3 and R_6 gave values of the dissociation constants K_R and K_R^0 and the allosteric constants L^0_A and L^0_B that are in good agreement with previous values estimated for the SMB model (Table 2) (*11*).

The cobalt-substituted hexamer shows a similar behavior (Figure 3C,D). When 4TFMB binds to the 2,7-DHN-stabilized form of the cobalt−insulin hexamer, the sample gives a 1D ^{19}F NMR spectrum consisting of a sharp peak located at 15.44 ppm corresponding to the free ligand and a broad envelope of resonances corresponding to the bound species with chemical shifts that vary with 2,7-DHN concentration, ranging from 19.02−18.83 ppm (Figure 3C). However, only a single Lorentzian was necessary to describe the shape of the bound peak (Figure 3D, black dots). The binding isotherm determined by measuring the changes in the d−d transitions of the absorption spectrum shows a dependence on concentration that is similar to the dependence of the ^{19}F peak area on concentration (Figure 3D, white dots). Both the ^{19}F NMR and UV/vis titrations were fitted using eq 2.

The ^{19}F NMR spectra of 3TFMB measured in the presence of the 2,7-DHN-stabilized zinc hexamer show the presence of a sharp peak with a chemical shift of 15.49 ppm corresponding to the free 3TFMB ligand and a broadened envelope, located between 16.7 and 17.0 ppm, corresponding to the bound ligand (data not shown). At every 2,7-DHN concentration, the envelope of bound peaks can be well-described by the sum of two Lorentzian-shaped curves with similar chemical shifts, amplitudes, and line widths. When the concentration of 3TFMB is held constant and in large excess over the zinc−insulin hexamer while the concentration of 2,7-DHN is varied (Figure 4A,B), the areas of the bound ^{19}F NMR peaks show very similar concentration dependencies, initially increasing and then tending toward constant values (Figure 4A). The apparent chemical shifts of both bound peaks move slightly upfield with essentially the same concentration dependence (Figure 4B). The sum of the two peaks (open triangles, Figure 4A) can be well-fitted by the equation for the formation of T_3R_3 species (eq 4). Comparisons with Figure 2 showed that the total area of these two peaks approaches a value that corresponds to a stoichiometry of one site per hexamer. The fitting of the curve to the SMB model gives values of K_R and K_R^0 that are consistent with published values for 2,7-DHN (*11*), and the values of the allosteric constants, L_0^A and L_0^B (Table 2) are in good agreement with the values obtained from the phenol titration for the same carboxylate with the Zn(II)-substituted hexamer.

^{19}F NMR Studies of Trifluorimethylbenzoate Binding to the Phenol-Stabilized Insulin Hexamer. When 4TFMB binds to the phenol-stabilized form of the zinc insulin hexamer, the complex gives a 1D ^{19}F NMR spectrum consisting of a relatively sharp peak located at approximately 15.44 ppm corresponding to the unbound ligand and an envelope of broadened spectral bands shifted downfield to the 16.1−16.4 ppm region, corresponding to the bound species (data not shown). This downfield spectral envelope is well-fitted by the assumption that it is dominated by two overlapping Lorentzian-shaped transitions with trace amounts of a third band (Figure 5A).

When the concentration of phenol is varied while holding the concentration of 4TFMB constant and in large excess over the zinc−insulin hexamer (Figure 5A), the area of one of the predominating bound peaks (open squares) initially increases, then decreases, and finally tends toward a constant, finite value, while the other peak (solid circles) follows a sigmoidal dependence. The area of the third peak (open

Table 2: Summary of Allosteric Parameters, L_0^A and L_0^B and Dissociation Constants K_R^0 and K_R Obtained by Fitting the Titration Data in Figures 3−7 to the SMB Model[a]

metal	HisB10 ligand	phenolic ligand	L_0^A	L_0^B	K_R (M)	K_R^0 (M)	figure[b]
Zn	3TFMB	2,7-DHN	271	1.37×10^6	1.97×10^{-4}	2.80×10^{-4}	4A
	3TFMB	phenol	257	1.37×10^6	2×10^{-4}	3.64×10^{-4}	5D
Zn	4TFMB	2,7-DHN	162	1.17×10^6	2.36×10^{-4}	2.86×10^{-4}	3B
	4TFMB	phenol	162	1.12×10^6	2×10^{-4}	3.64×10^{-4}	5A
Co	4TFMB	2,7-DHN	799	5×10^6	1.77×10^{-4}	2.86×10^{-4}	3D
	4TFMB	phenol	799	2.1×10^6	2×10^{-4}	3.64×10^{-4}	5B
Zn	4TFMC	2,7-DHN	735	2×10^6	1.90×10^{-4}	2.86×10^{-4}	6B,D
	4TFMC	phenol	735	1.72×10^6	2×10^{-4}	3.64×10^{-4}	6F
Zn	2TFMC	2,7-DHN	229	6.65×10^5	3.8×10^{-4}	2.75×10^{-4}	7B
	2TFMC	phenol	229	6.65×10^5	2×10^{-4}	3.64×10^{-4}	7D
Co	2TFMC	phenol	751	7.28×10^6	1.8×10^{-4}	4.08×10^{-4}	7F

[a] The parameters given in this table are estimated to have the following errors limits: L_0^A, ±42%; L_0^B, ±38%; K_R^0, ±12%; and K_R, ±24%, respectively. [b] Figure from which the parameters were obtained.

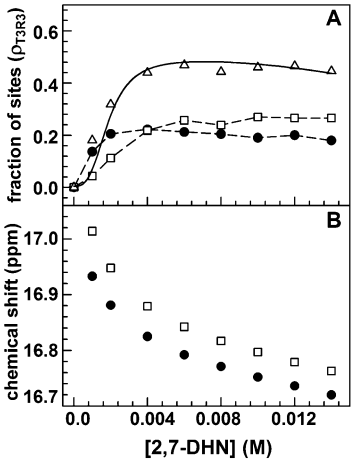

FIGURE 4: (A) ^{19}F NMR titration of the zinc hexamer with 2,7-DHN in the presence of 3TFMB. The bound envelope was fitted as two Lorentzian peaks at every 2,7-DHN concentration. Solid circles and open squares represent the calculated areas of the two peaks. Open triangles represent the sum of the two peaks assigned as the formation of the T_3R_3 species. The solid line is the best fitting to the SMB model (Scheme 1) to the expression for ρ_{T3R3} (eq 4). (B) Chemical shift dependence of the fitted 3TFMB bound peaks on the 2,7-DHN concentration in the presence of the zinc hexamer.

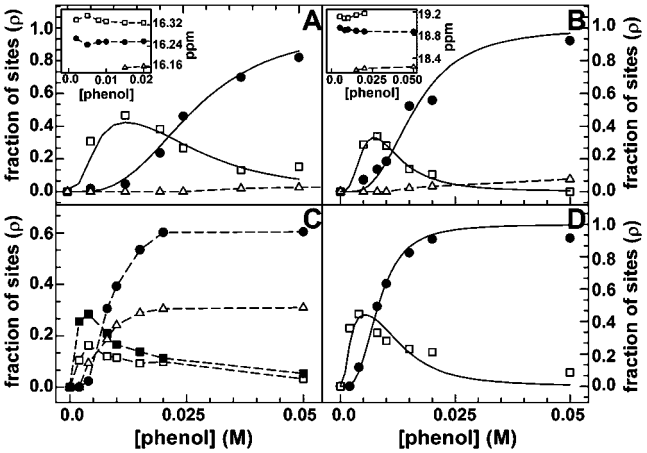

FIGURE 5: Phenol titration of the zinc (A) and cobalt (B) hexamers in the presence of 4TFMB. Peak areas for the bound species were calculated by fitting the bound envelope as a composition of three Lorentzian equations (eq 3). Assignments: open squares represent T_3R_3, solid circles represent R_6, and open triangles represent the third peak. Solid lines represent the best fitting of T_3R_3 and R_6 species of the SMB model using eqs 4 and 5. The chemical shift dependencies for the phenol titrations of the zinc and cobalt hexamers in the presence of 4TFMB are shown in the insets to panels A and B, respectively. (C) Phenol titration of the zinc hexamer in the presence of 3TFMB. Peak areas of the bound species were calculated by fitting the bound envelope as a sum of four Lorentzian equations. Assignments: solid and open squares represent two different modes for the binding of 3TFMB to T_3R_3; the solid circles and open triangles represent two alternative modes for the binding of 3TFMB to R_6. (D) Fitting of the phenol titration curves in panel C to the SMB model for the zinc hexamer in the presence of 3TFMB. Open squares represent the total amount of T_3R_3 (sum of open and solid squares in panel C); solid circles represent the total R_6 (sum of solid circles and open triangles in panel C). Solid lines represent the best fitting to the expressions for ρ_{T3R3} (eq 4) and ρ_{R6} (eq 5).

triangles) is not detected at subsaturating phenol concentrations and is present only in trace amounts at high concentrations (Figure 5A). The apparent chemical shifts of all three peaks were found to be essentially independent of the phenol concentration. When the same experiment was performed with the cobalt-substituted hexamer, similar dependencies were observed (Figure 5B). In both the Zn(II)− and Co(II)−insulin systems, the concentration dependencies of the two major peaks were well-described by the SMB model (eqs 4 and 5, solid lines), the equations for the formation and disappearance of T_3R_3 (white squares), and the sigmoidal formation of R_6 (black dots).

When 3TFMB binds to the phenol-stabilized form of the zinc insulin hexamer, the sample gives a 1D ^{19}F NMR spectrum consisting of a relatively sharp peak located at approximately 15.49 ppm corresponding to the unbound ligand and an envelope of broadened spectral bands shifted downfield corresponding to the bound species (Figure 1A). The chemical shift of the bound envelope changes as the phenol concentration is increased from 17.01−16.90 ppm. As shown in Figure 1B, the ^{19}F NMR signals arising from the binding of 3TFMB to the phenol-stabilized zinc−insulin hexamer required four Lorentzian-shaped curves to achieve a good fit of the spectrum. The chemical shifts of all four peaks move slightly upfield as the concentration of phenol is increased (Figure 1A). The dependencies of peak areas on the concentration of phenol are shown in Figure 5C. In Figure 5C, two of the resonances initially increase and then decrease (open squares and black squares), approaching zero area as the phenol concentration is increased. The areas of the peak designated by black dots exhibit a lag phase, then increase with a sigmoidal dependence, reaching a value of about 60% of the total. The species designated by the open

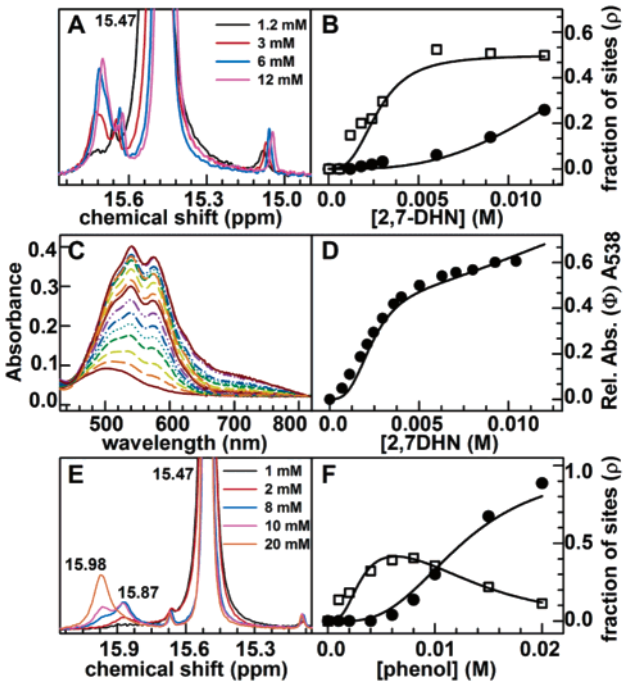

FIGURE 6: (A) 1D ^{19}F NMR spectra of 4TFMC in the presence of the zinc hexamer at different 2,7-DHN concentrations. (B) Plot of relative areas taken from panel A for the bound peaks fitted as two Lorentzians (eq 3). Assignments: open squares, T_3R_3; solid circles, R_6. Solid lines represent the best fitting of T_3R_3 and R_6 species to the SMB model (Scheme 1) using eqs 4 and 5. (C) Absorbance spectra of the cobalt−insulin hexamer in the presence of 4TFMC versus increasing concentrations of 2,7-DHN. (D) Titration isotherm obtained by varying the 2,7-DHN concentration measured as the absorbance increase at 538 nm. The solid line represents the best fitting of the fraction of sites (ρ) to the SMB model using eq 2. (E) 1D ^{19}F NMR spectra of 4TFMC measured in the presence of the zinc hexamer at different phenol concentrations. The free peak of 4TFMC has a chemical shift of 15.47 ppm. The bound species exhibits an envelope of two peaks, with chemical shifts varying from 15.87 at 1 mM phenol to 15.98 at 20 mM phenol. (F) Phenol titration of the zinc hexamer in the presence of 4TFMC (data taken from panel E). Assignments: open squares, T_3R_3; black circles, R_6. Solid lines represent the best fitting of the peak areas to the expressions for ρ_{T3R3} (open squares, eq 4) and ρ_{R6} (solid dots, eq 5), respectively.

triangles follows a similar behavior, reaching a value of about 30% of the total. The areas of the two peaks represented by open squares and solid squares were summed together (open squares in Figure 5D). The dependence of the resulting new curve is well-described by eq 4 (solid line). The curve resulting from the sum of the areas of the peaks described by the solid circles and open triangles in Figure 5C is represented by black dots in Figure 5D. The total area of these peaks approaches a value that corresponds to a stoichiometry of two sites per hexamer, and the dependency on the phenol concentration is well-described by the SMB model (eq 5, solid line).

^{19}F NMR Studies of Trifluorimethylcinnamate Binding to the 2,7-DHN and Phenol-Stabilized Insulin Hexamers. The ^{19}F NMR spectra of 4-trifluoromethylcinnamate (4TFMC) (Figure 6A) bound to the 2,7-DHN-stabilized zinc−insulin hexamer show a free peak at 15.47 ppm and an envelope consisting of two broadened overlapping resonances in the 15.6−15.8 ppm region that slightly overlap with the ^{13}C satellite peak of the free ligand at 15.64 ppm. Although more difficult to quantify, the plots of peak area (Figure 6B) versus 2,7-DHN concentration indicate that one species (open squares) predominates, while the second species (black dots) lags behind, and then becomes increasingly significant in area at higher concentrations of 2,7-DHN. The shape is consistent with the initial portion of a sigmoidal curve. The concentration dependence of the predominant peak (open squares) was fitted to the equation describing the formation of T_3R_3 (SMB model, eq 4, solid line), while the concentration dependence of the second peak (black circles) was well-described by the equation for the appearance of R_6 (eq 5) (solid line). As observed with the other trifluoromethyl-substituted aromatic carboxylates, the chemical shifts of each of the two resonances move slightly upfield as the concentration of 2,7-DHN is increased (data not shown).

Figure 6C shows the dependence of the UV/vis absorption spectrum of the d−d transitions of the cobalt−insulin hexamer under conditions where the concentration of 4TFMC is held constant and in large excess over the hexamer concentration while the concentration of 2,7-DHN is varied. Under similar conditions with *p*-aminobenzoate as the ligand for the HisB10 anion site (*11*), the binding of 2,7-DHN shifts the hexamer from the T_6 state to predominantly T_3R_3. The resulting titration curve for 4TFMC (Figure 6D) shows that the appearance of the R-state species is slightly sigmoidal under these conditions. The titration curve was fitted using the SMB model (eq 2) (solid line) for the appearance of T_3R_3, giving values of the allosteric parameters that are in good agreement with the ^{19}F NMR titrations shown in Figure 6A and with previous data (Table 2) (*11*).

The binding of 4TFMC to the phenol-stabilized zinc−insulin hexamer gives a ^{19}F NMR spectrum for the bound species consisting of two broadened and overlapping peaks (Figure 6E). When the phenol concentration is varied, the peak area for the resonance designated by open squares initially increases and then decreases. This curve was fitted using the equation for the formation and the decay of T_3R_3 upon phenol binding (eq 4). The dependence of the peak area for the resonance designated by filled circles follows a sigmoidal isotherm and was fitted by the equation for the formation of R_6 (eq 5) (Figure 6F) (solid line). The chemical shifts of both resonances are essentially independent of the phenol concentration (Figure 6E).

The ^{19}F NMR spectra of 2-trifluoromethylcinnamate (2TFMC) bound to the 2,7-DHN-stabilized zinc−insulin hexamer show a free peak at 19.14 ppm and a broadened envelope of bound signal(s) at about 20.0 ppm (Figure 7A). The bound envelope appeared to be too broad to be a single peak and was therefore fitted as two peaks at every 2,7-DHN concentration. When the areas of the two putative peaks are plotted versus the 2,7-DHN concentration, two binding isotherms are obtained with similar hyperbolic shapes (Figure 7B). The chemical shifts of the two putative peaks move slightly upfield as the 2,7-DHN concentration is increased (Figure 7A). The sum of the areas of these peaks (open triangles) can be adequately fitted by eq 4, the equation for the stabilization of T_3R_3 species (solid curve).

The ^{19}F NMR studies of the binding of 2TFMC to the phenol-stabilized zinc−and cobalt−insulin hexamers (Figures 7C and 7D and Figures 7E and 7F, respectively) show that, in each system, the spectrum of bound 2TFMC consists of a broadened envelope. In the Zn^{2+} system, the envelope likely consists of two overlapping peaks. In the Co^{2+} system, the

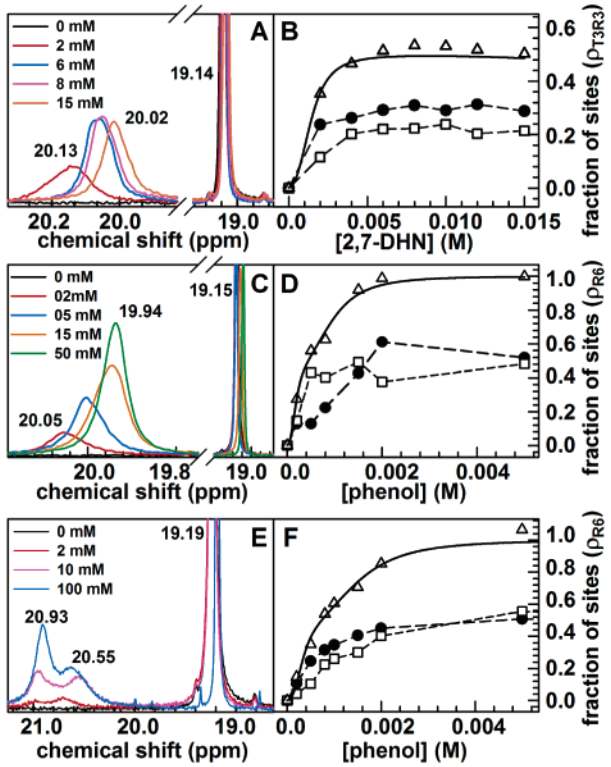

FIGURE 7: (A) 1D ^{19}F NMR spectra of 2TFMC measured in the presence of the zinc−insulin hexamer at different 2,7-DHN concentrations. (B) The spectra in panel A were fitted with the assumption that the bound envelope consists of two Lorentzian peaks (open squares and solid circles), each corresponding to the binding of 2TFMC to T_3R_3. The solid line represents the best fitting of the summed areas (open triangles) to the expression for the T_3R_3-state species (SMB model, eq 4). (C) 1D ^{19}F NMR spectra of 2TFMC measured in the presence of the zinc hexamer at different phenol concentrations. (D) The envelope of bound species in panel C was fitted assuming it consists of two Lorentzian peaks (open squares and solid circles) (eq 3). The solid line represents the best fitting of the sum of these areas (open triangles) to the expression for the total R-species (SMB model, eq 2). (E) 1D ^{19}F NMR spectra of 2TFMC measured in the presence of the cobalt hexamer at different phenol concentrations. (F) The envelope of bound resonances in panel E was assumed to consist of two peaks and was fitted at every phenol concentration as a combination of two Lorentzian curves (open squares and solid circles) (eq 3). Open triangles represent the sum of these peaks, and the solid line represents the best fitting of the sum of these peak areas (open triangles) to the expression for the total R-species (ρ) (SMB model, eq 2).

envelope clearly consists of two peaks. It was found that each of these envelopes could be well-described by two Lorentzians, with similar dependencies of the chemical shift, the peak area, and the line width on the concentration of phenol. The sum of the two putative bound peaks for the titration of the Zn(II)-substituted insulin hexamer and the sum of the two peaks of the Co(II)-substituted insulin hexamer (open triangles in figures 7D and 7F, respectively) both give titration curves that are well-fitted by the equation for the dependence of the R-state on phenol binding according to the SMB model (eq 2, solid line). The values obtained for K_R and K_R^0 for these phenol titrations are in very good agreement with the values obtained for other phenol titrations involving different mono anions bound to the metal site (Table 2) (*11*, *13*).

Competition between Phenolate Ion and the Aromatic Carboxylates. The K_{Dapp} values reported by Huang et al. (*29*)

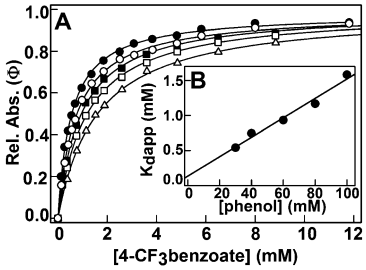

FIGURE 8: (A) UV/vis titrations for the binding of 4TFMB to the cobalt hexamer at different concentrations of phenol. Phenol concentrations: 30 mM (solid circles), 40 mM (open circles), 60 mM (solid squares), 80 mM (open squares), and 100 mM (open triangles). Solid lines represent the fitting of each concentration set to eq 1 to determine K_{Dapp} (see Materials and Methods). (B) Dependence of K_{Dapp} on phenol concentration. The solid line represents the best fit of the K_{Dapp} values obtained in panel A to eq 11. The extrapolated values for K_{phenol} and K_D are 9.7 mM and 0.14 mM, respectively.

for the binding of organic carboxylates and the values reported herein for the trifluoromethyl benzoates and cinnamates are measured in competition with the binding of phenolate ion to the HisB10 sites. Consequently, the apparent dissociation constants measured for these carboxylate ligands are attenuated by this competition. To estimate the effects of this competition on the apparent affinities of the carboxylate ligands, the dependence of the 4TFMB K_{Dapp} value for the cobalt hexamer was measured at different phenol concentrations (Figure 8A). If the inhibition by phenolate ion is a strictly competitive process, then the equation for competitive inhibition of ligand binding (eq 11) predicts that the plot of K_{Dapp} versus [phenol] will be linear.

$$K_{Dapp} = [((1 + [\text{phenol}])/K_{phenolate})K_D] \qquad (11)$$

In eq 11, K_{Dapp} is the apparent dissociation constant of the organic carboxylate, $K_{phenolate}$ is the apparent dissociation constant for the binding of phenolate ion to the HisB10 site at pH 8.0 and 25 °C, and K_D is the intrinsic dissociation constant of the organic carboxylate. Figure 8B shows that the dependence of K_{Dapp} on [phenol] is linear. According to this treatment, $K_{phenolate}$ is 9.7 mM at pH 8.0, and the intrinsic dissociation constant for 4TFMB is K_D = 0.14 mM. This result shows that, under the experimental conditions used in this work where [phenol] = 100 mM and pH = 8.0, competition with phenolate ion weakens the apparent affinities of the carboxylate ligands by about 10-fold. Table 1 summarizes the experimentally determined values of K_{Dapp} and the values of K_D calculated for the carboxylate ligands used in this study.

DISCUSSION

The regulation of protein function via allosteric interactions continues to be a challenging and intriguing area of investigation. The SMB model for half-site reactivity and negative cooperativity is based on the assumption of inherent symmetry and asymmetry of oligomeric proteins. This model is capable of providing quantitative descriptions of mixed positive and negative heterotropic and homotropic interactions through a symmetry−asymmetry-based cooperativity mechanism that relies on symmetry constraints.

Allosteric behavior is a dynamic process involving the switching of the oligomeric protein between alternative

conformation states. High-resolution structures of allosteric proteins determined via X-ray crystallography have made enormously important contributions to our knowledge of the structural origins of allosteric behavior. This structural database for the insulin hexamer identifies three global conformations, designated T_6, T_3R_3, and R_6 (*6*). Previous investigations have shown that, when appropriately tailored to the insulin hexamer, the three-state SMB model provides excellent agreement between allosteric behavior in solution and the X-ray crystal structures of the hexamer (*10*−*13*). However, the details of tertiary and quaternary subunit structure, the number of relevant conformation states in solution, and the kinetics of the interconversions remain of central importance to the understanding of allosteric regulation. Therefore, we have extended our solution studies of the allosteric behavior of the insulin hexamer to detect and quantify the number and distribution of conformation states present in the insulin system.

The Trifluoromethyl-Substituted Ligands Bind to the HisB10 Pockets of T_3R_3 and R_6. The slow and intermediate exchange rates among free and bound states, together with the high sensitivity to chemical environment of the trifluoromethyl-substituted ligands used in this study, gives rise to an envelope of resonances for the bound states that is well-separated from the free peaks. For several of the ligand−protein systems investigated, the ^{19}F NMR spectra establish that the time scale for exchange among bound states also is slow to intermediate with respect to the NMR time scale and, therefore, gives a broadened but overlapping envelope of resonances for the bound species. In some instances, the individual peaks for bound species are clearly distinguishable (Figures 1, 2, 4−6, and 7E); in other instances, the broadened structure of the bound envelope is indicative of more than one peak in intermediate to slow exchange (Figures 3 and 7A,C). Gerig's laboratory has extensively documented similar behavior for the binding of fluorinated ligands to protein sites (*23*, *25*, *32*−*36*). In our experiments, the bound resonances correspond to protein−ligand complexes with different chemical shifts, reflecting the high sensitivity of fluorine chemical shifts to small differences in microenvironment (*24*) (Figures 1−7), and these overlapping resonances can be decomposed into individual peaks by fitting to Lorentzian-shaped transitions.

To determine if the fluorinated carboxylates bind specifically to the HisB10 sites of the R-state hexamer species, the stoichiometry of binding was determined both by ^{19}F NMR spectroscopy for the zinc−insulin hexamer (Figure 2A) and by UV/vis spectroscopy for the cobalt−insulin hexamer (Figure 2B). The results establish that two carboxylate molecules bind to the insulin complex in the R_6 state, whereas only a single carboxylate molecule binds to the T_3R_3 state (Figure 2C,D), one per R_3 trimeric unit in each hexamer. The changes in the absorption spectrum of the Co(II)-substituted hexamer verify that binding occurs at the HisB10 pockets and involves inner sphere coordination of the ligand carboxylate in a distorted 5-coordinate complex (*17*, *21*, *29*, *30*, *37*). The only evidence found indicating the trifluoromethyl-substituted ligands may in one instance also bind to another site on the protein is the minor peak (Figure 5A, open triangles) observed in the binding of 4TFMB to the phenol-stabilized hexamer. The area of this peak corresponds to only a trace amount of bound ligand and a stoichiometry far less than 1:1. Therefore, we have neglected this species in our analysis.

The Dynamics of Ligand Binding Imply That Aromatic Carboxylates Bind to Capped HisB10 Pockets. Since the affinities of these ligands range from 10−100 μM (Table 1), we were surprised to find the exchange between free and bound states to be slow. If binding occurs at, or near, the diffusion limit, then the off rates for these ligands should be in the range of 10^3−10^5 s^{-1}. From analysis of the line widths of the ^{19}F NMR resonance of unbound 3TFMB (Figure 1C), the rate of ligand dissociation, k_{off}, was found to be slower than the diffusion-limited value by at least 3 orders of magnitude. The value obtained, 2.22 ± 0.05 s^{-1}, is similar to the value reported for another aromatic carboxylate, 3-nitro-4-hydroxybenzoate (4.13 s^{-1}) (*21*).

In agreement with the conclusions of Olsen et al. (*21*), we also conclude that the slow off rate implies that dissociation is limited by a protein conformational transition. The R_6 structure with phenolate ion coordinated to the HisB10 site published by Smith and Dodson (*38*) shows that the N-terminal residues of the B-chain can form a cap over the entrance to the HisB10 site when phenolate ion is bound. The proposal of a capped HisB10 site for the aromatic carboxylate complexes helps to provide a reasonable explanation for the unexpectedly slow off rate for the ligand, provided the transition to an open conformation is rate-determining.

The Ligand Binding Isotherms Support the SMB Allosteric Model for Insulin Behavior. When the phenolic ligand is 2,7-DHN, the two Lorentzians required to fit the 3TFMB envelope of peaks bound to the Zn(II) hexamer show similar dependencies on the concentration of 2,7-DHN. When the sum of the areas of these two Lorentzians is plotted versus the concentration of 2,7-DHN (Figure 4A), the resulting curve is consistent with the conversion of T_6 to T_3R_3. The 4TFMB (Figure 3) and 4TFMC (Figure 6B) systems involving 2,7-DHN as the phenolic ligand behave similarly. This behavior is consistent with earlier experiments demonstrating the apparent half-site reactivity and negative cooperativity in the binding of 2,7-DHN (*10*, *11*) and provides additional evidence strongly indicating that the insulin hexamer is well-described by the SMB model.

For the phenol stabilized hexamers, the areas of the two dominating, resolved Lorentzians obtained with 4TFMB (Figure 5A,B), 3TFMB (Figure 5D), or 4TFMC (Figure 6F) exhibit phenol concentration dependencies, both for the Zn(II) or the Co(II) systems, that provide strong evidence in favor of a mechanism wherein T_6 is sequentially converted to T_3R_3, followed by the conversion of T_3R_3 to R_6. The concentration dependencies presented in Figures 5 and 6 can be fitted to the SMB model (solid curves), yielding the allosteric constants, L_0^A and L_0^B, and dissociation constants, K_R^0 and K_R, given in Table 2. In each instance, the values obtained are in good agreement with previously estimated values (*10*, *11*, *13*). According to the SMB model (Scheme 1), the parameters L_0^A and L_0^B describe the thermodynamics for the interconversion of a set of preexisting states, T_6, T_3R_3, and R_6, and exclude other species, such as T_5R_1, T_4R_2, T_2R_4, T_1R_5, and species that are made up of heterogeneous trimeric units (e.g., a T_2R_1 unit combined with a T_1R_2 unit). Because the model, as presented in Scheme 1, explicitly takes into account the influence of ligand binding at the phenolic

Scheme 2: Structure of the Phenol-Stabilized R_6 Hexamer (Accession File 1ZNJ.PDB) (*39*) Viewed along the 3-Fold Symmetry Axis with Either 4TFMB (A) or 3TFMB (B and C) Modeled into One of the HisB10 Sites in Place of the Ligand Present in the PDB File[a]

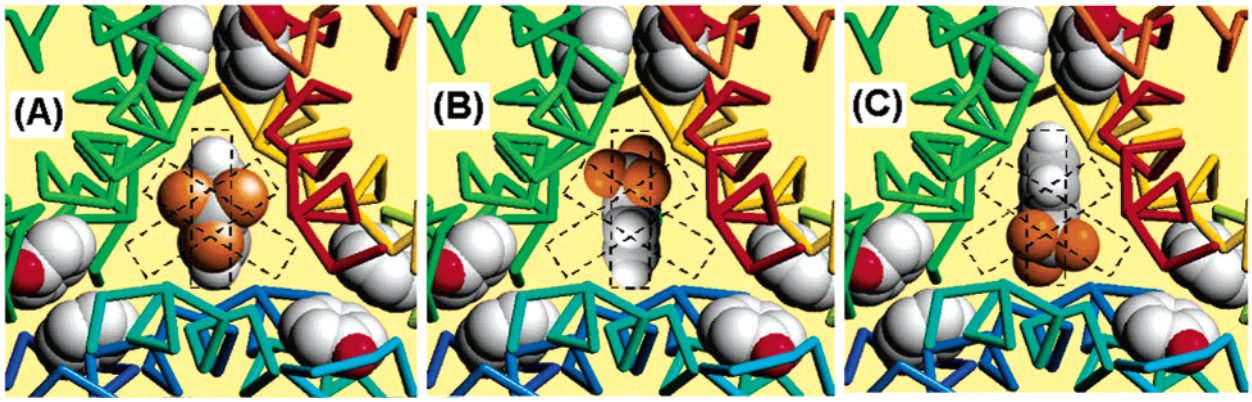

[a] Binding of 4TFMB and 3TFMB was modeled assuming the ligand carboxylate is coordinated to the HisB10 metal ion and that the planar organic ring of the ligand is oriented along the 3-fold symmetry axis with one edge wedged against a dimer−dimer interface and the other against a monomer−monomer interface. Because of the 3-fold symmetry of the hexamer, there are three equivalent, but overlapping, positions (dashed rectangles) for the ligand at each HisB10 site. The models in panels B and C show alternative orientations of 3TFMB resulting from a 180° flip of the ring. As is evident from comparison of these models, the 180° flip places the CF_3 group in two different protein microenvironments, whereas a 180° flip in model A will not alter the microenvironment of the 4TFMB CF_3 group. 4TFMB, 3TFMB, and the six phenols are shown in spacefilling mode with CPK coloring (C, gray; H, white; O, red; F, gold). The hexamer is shown in backbone representation with each insulin chain assigned a different color (the insulin molecules of the dimeric units are, respectively, light and dark green, yellow and orange, light blue and dark blue).

pockets but not at the HisB10 sites, the apparent values of L_0^A and L_0^B are influenced by ligand binding to the HisB10 sites but not by ligand binding to the phenolic pockets. Therefore, provided the same HisB10 ligand is used and its total concentration is held constant, the model predicts that the values of L_0^A and L_0^B will be unaffected by the structure of the ligand bound to the phenolic pocket. Similarly, provided that the same phenolic ligand is used, different HisB10 ligands will alter the values of L_0^A and L_0^B but will not alter the values of K_R^0 and K_R (*10*−*13*). Inspection of Table 2 shows that these predictions are satisfied.

The Binding of 3TFMB and 2TFMC Populate Two Slowly Exchanging Binding Modes within the Same R-State Site, While 4TFMB and 4TFMC Do Not. In contrast to the behavior of 4TFMB (Figure 3) and 4TFMC (Figure 6B), the ^{19}F NMR spectra for the binding of both 3TFMB (Figures 2C and 4A) and 2TFMC (Figure 7B) to the 2,7-DHN-stabilized T_3R_3 hexamer each show envelopes that appear to consist of two resonances for the bound species. In both systems, the dependencies of the areas of these two peaks on the concentration of 2,7-DHN show essentially the same curve shape. For both the 3TFMB (Figure 4A) and 2TFMC (Figure 7B) systems, the amplitudes of the two peaks are very similar. In each instance, since the fraction of R_6 formed is negligible, we conclude that both curves represent the conversion of T_6 to T_3R_3 (eq 4). In agreement with this conclusion, the plots of the sum of the areas of the two peaks are well-fitted by the SMB model equation for the sum of the R-sate species (solid curves), and the values of the allosteric parameters L_0^A, L_0^B, K_R^0, and K_R obtained (Table 2) are consistent with previously determined values (*10*, *11*).

It then follows that the two peaks originating from bound species in the 3TFMB spectra (Figures 2C and 4A) and 2TFMC (Figure 7B) each arise from two different binding modes within the same R_3 binding site, corresponding to two different chemical shift environments for the CF_3 group. Similar behavior has been reported for the binding of fluorinated ligands to other protein sites (*23*, *26*, *32*, *35*). The HisB10 pocket of the R_3 unit in T_3R_3 is a site with 3-fold symmetry (Schemes1 and 2). When viewed along the 3-fold symmetry axis, the HisB10 site has a roughly triangular cross section imposed by the 3-helix bundle that creates the amphipathic binding site.

As depicted in Scheme 2, the dimensions of the site can accommodate an aromatic carboxylate such as 4TFMB or 4TFMC in one of three identical, but overlapping, orientations (dashed rectangles). In Scheme 2A, 4TFMB is modeled into the site with the assumption that the CF_3 group resides on the 3-fold symmetry axis of the hexamer. Since the rotation of a CF_3 group about the C−C single bond to the ring almost certainly is rapid, each of the three fluorine atoms will sample an identical, averaged microenvironment, giving a single, bound resonance.

If the CF_3 group of 4TFMB resides close to, but not exactly on, the 3-fold symmetry axis, an 180° flip will give two different chemical environments. However, if the deviation from the 3-fold axis is small, there may not be a sufficient difference in chemical shift to allow detection of the two binding modes. Alternatively, if flipping is rapid relative to the NMR time scale, then a single resonance with an averaged chemical shift would be observed. Our experiments show only a single bound resonance assigned to the 2,7-DHN-stabilized T_3R_3 complexes with 4TFMB (Figure 3A−D) and with 4TFMC (Figure 6B). These results are consistent with any of the three foregoing arguments. Consequently, in the 4TFMB and 4TFMC systems, either the steric clashing is reduced, giving a flipping rate that is rapid and therefore a single peak, or the CF_3-group resides on or near the 3-fold symmetry axis and there is insufficient difference in chemical shift to allow detection of the two binding modes.

The situation is different for 3TFMB and 2TFMC. When modeled into the HisB10 site (Scheme 2B,C), the CF_3 groups of 3TFMB and 2TFMC do not reside on or near the 3-fold symmetry axis. When the aromatic ring is flipped by 180°, then the CF_3 groups sample two different microenvironments

(compare Scheme 2B with Scheme 2C). Provided that the 180° flip is slow and that the difference in chemical shift is detectable, then the ^{19}F NMR spectrum of the bound species will consist of two resonances. Since two resonances are observed when 3TFMB or 2TFMC bind to T_3R_3 (Figures 4 and 7A,B), we conclude that the flipping rate is slowed by the steric clashing of the CF_3 group with the walls of the site, giving two peaks. Gerig's ^{19}F NMR work provides ample precedent for slow ring flipping rates in protein ligand complexes (*23*, *26*, *32*, *35*).

The phenol titration of 3TFMB (Figures 1 and 5C) shows four resonances. Two resonances (open squares and filled squares) exhibit the pattern characteristic of the T_6 to T_3R_3 transition, while the other two (filled circles and open triangles) have sigmoidal shapes and correspond to the transformation of T_3R_3 to R_6. When summed together, the two resonances assigned to T_3R_3 are well-fitted by the equation describing the transition from T_6 to T_3R_3 (open squares in Figure 5D), while the sum of the two resonances assigned to R_6 (filled circles in Figure 5D) gives a curve that is well-described by the equation for the formation of R_6 state. Therefore, we propose that the peaks corresponding to open and solid squares in Figure 5C arise from two different modes of binding to the T_3R_3 complex, with the same origins as depicted in Scheme 2B,C, while the peaks corresponding to solid circles and open triangles describe two different modes for the binding of 3TFMB to the R_6 complex, just as proposed for the two peaks detected when the phenolic ligand is 2,7-DHN.

Finally, the titrations of the Zn(II)- and Co(II)-substituted hexamers when 2TFMC is the HisB10 ligand (Figure 7D and 7F) each show two peaks of similar amplitudes exhibiting similar dependencies on the concentration of phenol. When the areas of the two peaks are summed, the resulting titrations are well-fitted by the assumption that the curves represent the sum of the R-state species (2TFMC bound to T_3R_3 and to R_6). These titrations suggest that the binding of 2TFMC decreases L_0^B such that the accumulation of T_3R_3 is greatly reduced. If this analysis is correct, then the two observed resonances also logically arise from two modes of binding to R_6, as proposed in Scheme 2.

In summary, the CF_3-substituted ligands for the HisB10 site presented in this study provide ^{19}F NMR probes that are sensitive indicators of subunit conformation in the insulin hexamer. These experiments show that, when coupled to slow exchange between free and bound states, the high sensitivity of the fluorine chemical shifts of these ligands to the microenvironment provide spectroscopic signatures that distinguish between the T_3R_3 and R_6 conformational states of the insulin hexamer. Heretofore, it has not been possible to distinguish between these states by optical spectroscopy. While ^{1}H NMR has given evidence for T_3R_3 and R_6 conformational states exhibiting different ^{1}H spectroscopic signatures (*1*, *9*−*11*, *17*), the ^{1}H signatures have been of limited use, both in identifying quaternary states and in quantifying the ligand binding isotherms for the interconversion of quaternary states in the insulin hexamer system. Through documentation of the interconversion of T_6, T_3R_3, and R_6 species, the ^{19}F NMR results presented in this work contribute strong additional experimental evidence for the applicability of the SMB model as a description of the mechanism of insulin allosteric behavior.

ACKNOWLEDGMENT

We thank Niels C. Kaarsholm for his interest and insightful advice concerning these studies, and we thank Novo Nordisk for a generous gift used to support this work.

REFERENCES

1. Roy, M., Brader, M. L., Lee, R. W.-K., Kaarsholm, N. C., Hansen, J., and Dunn, M. F. (1989) Spectroscopic signatures of the T to R conformational transition in the insulin hexamer, *J. Biol. Chem. 264*, 19081−19085.
2. Rahuel-Clermont, S., French, C. A., Chou, C. I., Kaarsholm, N. C., and Dunn, M. F. (1997) Mechanisms of stabilization of the insulin hexamer through allosteric ligand interactions, *Biochemistry 36*, 5837−5845.
3. Steiner, D. F., Peterson, J. D., Tager, H. S., Emdin, S., Ostberg, Y., and Falkmer, S. (1973) Comparative aspects of proinsulin and insulin structure and biosynthesis, *Am. Zool. 13*, 591−604.
4. Blundell, T., Dodson, G., Hodgkin, D., and Mercola, D. (1972) Insulin: the structure in the crystal and its reflection in chemistry and biology, *Adv. Protein Chem. 26*, 279−402.
5. Bailyes, E. M., Guest, P. C., and Hutton, J. C. (1992) Insulin Synthesis, in *Insulin: Molecular Biology to Pathology* (Ashcroft, F. M., and Ashcroft, S. J. H., Eds) pp 64−92, Oxford University Press, New York.
6. Kaarsholm, N. C., Ko, H. C., and Dunn, M. F. (1989) Comparison of solution structural flexibility and zinc binding domains for insulin, proinsulin, and mini-proinsulin, *Biochemistry 28*, 4427−4435.
7. Brader, M. L., and Dunn, M. F. (1991) Insulin hexamers: new conformations and applications, *Trends Biochem. Sci., 16*, 341−345.
8. Choi, W. E., Brader, M. L., Aguilar, V., Kaarsholm, N. C., and Dunn, M. F. (1993) The allosteric transition of the insulin hexamer is modulated by homotropic and heterotropic interactions, *Biochemistry 32*, 11638−11645.
9. Brzovic, P. S., Choi, W. E., Borchardt, D, Kaarsholm, N. C., and Dunn, M. F. (1994) Structural asymmetry and half-site reactivity in the T to R allosteric transition of the insulin hexamer, *Biochemistry 33*, 13057−13069.
10. Bloom, C. R., Choi, W. E., Brzovic, P. S., Ha, J. J., Huang, S. T., Kaarsholm, N. C., and Dunn, M. F. (1995) Ligand binding to wild-type and E-B13Q mutant insulins; a three-state allosteric model system showing half-site reactivity, *J. Mol. Biol. 245*, *324*−*330*.
11. Bloom, C. R., Heymann, R., Kaarsholm, N. C., and Dunn, M. F. (1997) Binding of 2,6- and 2,7-dihydroxynaphthalene to wild-type and E-B13Q insulins: dynamic, equilibrium, and molecular modeling investigations, *Biochemistry 36*, 12746−12758.
12. Bloom, C. R., Kaarsholm, N. C., Ha, J. J., and Dunn, M. F. (1997) Half-site reactivity, negative cooperativity, and positive cooperativity: quantitative considerations of a plausible model, *Biochemistry 36*, 12759−12765.
13. Bloom, C. R., Wu, N., Dunn, A., Kaarsholm, N. C., and Dunn, M. F. (1998) Comparison of the allosteric properties of the Co(II)- and Zn(II)-substituted insulin hexamers, *Biochemistry 37*, 10937−10944.
14. Derewenda, U., Derewenda, Z., Dodson, E. J., Dodson, G. G., Reynolds, C., D., Smith, G., D., Sparks, C., and Swensen, D. (1989) Phenol stabilizes more helix in a new symmetrical zinc insulin hexamer, *Nature 338*, 594−596.
15. Smith, G. D., Swenson, D. C., Dodson, E. J., Dodson, G. G., and Reynolds, C. D. (1984) Structural stability in the 4-zinc human insulin hexamer, *Proc. Natl. Acad. Sci. U.S.A. 81*, 7093−7097.
16. Ciszak, E., and Smith, G. D. (1994) Crystallographic evidence for dual coordination around zinc in the T_3R_3 human insulin hexamer, *Biochemistry 33*, 1512−1517.
17. Brader, M. L., Kaarsholm, N. C., Lee, R. W.-K., and Dunn, M. F. (1991) Characterization of the R-state insulin hexamer and its derivatives. The hexamer is stabilized by heterotropic ligand binding interactions, *Biochemistry 30*, 6636−6645.
18. Whittingham, J. L., Chaudhuri, S., Dodson, E. J., Moody, P. C. E., and Dodson, G. G. (1995) X-ray crystallographic studies on hexameric insulins in the presence of helix-stabilizing agents, thiocyanate, methylparaben, and phenol, *Biochemistry 34*, 15553−15563.

19. Bentley, G. A., Brange, J., Derewenda, Z., Dodson, E. J., Dodson, G. G., Markussen, J., Wilkinson, A. J., Wollmer, A., and Xiao, B. (1992) Role of B13 Glu in insulin assembly. The hexamer structure of recombinant mutant (B13 Glu → Gln) insulin, *J. Mol. Biol. 228*, 1163−1176.
20. Baker, E. N., Blundell, T. L., Cutfield, J. F., Cutfield, S. M., Dodson, E. J., Dodson, G. G., Hodgkin, D. C., Hubbard, R. E., Isaacs, N. W., Reynolds, C. D., Sakabe, K., Sakabe, N., and Vijayan, N. M. (1988) The structure of 2Zn pig insulin crystals at 1.5 Å resolution, *Philos. Trans. R. Soc. London, Ser. B 319*, 369−456.
21. Olsen, H. B., Leuenberger-Fisher, M. R., Kadima, W., Borchardt, D., Kaarsholm, N. C., and Dunn, M. F. (2003) Structural signatures of the complex formed between 3-nitro-4-hydroxybenzoate and the Zn(II)-substituted R_6 insulin hexamer, *Protein Sci. 12*, 1902−1913.
22. Seydoux, F., Malhotra, O. P., and Bernhard, S. A. (1974) Half-site reactivity, *CRC Crit. Rev. Biochem. 2*, 227−257.
23. Dugad, L. B., Cooley, C. R., and Gerig, J. T. (1989) NMR studies of carbonic anhydrase-fluorinated benzenesulfonamide complexes, *Biochemistry 28*, 3955−3960.
24. Gregory, D. H., and Gerig, J. T. (1991) Prediction of fluorine chemical shifts in proteins, *Biopolymers 31*, 845−858.
25. Sylvia, L. A., and Gerig, J. T. (1995) NMR studies of the alpha-chymotrypsin-(*R*)-1-acetamido-2-(4-fluorophenyl)ethane-1-boronic acid complex at pH 7, *Biochim. Biophys. Acta 1252*, 225−232.
26. Sylvia, L. A., and Gerig, J. T. (1993) NMR studies of the alpha-chymotrypsin-(*R*)-1-acetamido-2-(4-fluorophenyl)ethane-1-boronic acid complex, *Biochim. Biophys. Acta 1163*, 321−334.
27. Lau, E. Y., and Gerig, J. T. (1997) Effects of fluorine substitution on the structure and dynamics of complexes of dihydrofolate reductase (*Escherichia coli*), *Biophys. J. 73*, 1579−1592.
28. Storm, M. C., and Dunn, M. F. (1985) The Glu(B13) carboxylates of the insulin hexamer form a cage for Cd^{2+} and Ca^{2+} ions, *Biochemistry 24*, 1749−1756
29. Huang, S. T., Choi, W. E., Bloom, C. R, Leuenberger, M., and Dunn, M. F. (1997) Carboxylate ions are strong allosteric ligands for the HisB10 sites of the R-state insulin hexamer, *Biochemistry 36*, 9878−9888.
30. Brader, M. L., Kaarsholm, N. C., Harnung, S. E., and Dunn, M. F. (1997) Ligand perturbation on a pseudotetrahedral Co(II)(His)-3L site. A magnetic circular dichroism study of the Co(II)-substituted insulin hexamer, *J. Biol. Chem. 272*, 1088−1094.
31. Lian, L.-Y., and Roberts, G. C. K. (1996) Effects of chemical exchange on NMR spectra, in *NMR of Macromolecules: A Practical Approach* (Roberts, G. C. K., Rickwood, D., and Hames, B. D., Eds.), pp 152−182, Oxford University Press, Oxford, U.K.
32. Ando, M. E., Gerig, J. T., Luk, K. F., and Roe, D. C. (1980) Evidence for multiple forms of *p*-trifluoromethylbenzenesulfonyl-alpha-chymotrypsin, *Can. J. Biochem. 58*, 427−433.
33. Ando, M. E., and Gerig, J. T. (1982) Reactions of alpha-chymotrypsin with 4-(trifluoromethyl)-alpha-bromoacetanilide, *Biochemistry 21*, 2299−2304.
34. Kairi, M., Keder, N. L., and Gerig, J. T. (1990) Conformations of *N*-(2-fluorophenyl)-*N*-phenylcarbamoyl-alpha-chymotrypsin, *Arch. Biochem. Biophys. 279*, 305−314.
35. Kairi, M., and Gerig, J. T. (1990) Conformational dynamics in fluorophenylcarbamoyl-alpha-chymotrypsins, *Biochim. Biophys. Acta 1039*, 157−170.
36. Jacobson, A. R., and Gerig, J. T. (1991) Structure and dynamics of alpha-chymotrypsin-*N*-trifluoroacetyl-4-fluorophenylalanine complexes, *J. Biomol. NMR 1*, 131−144.
37. Ferrari, D., Diers, J. R., Bocian, D. F., Kaarsholm, N. C., and Dunn, M. F. (2001) Raman signatures of ligand binding and allosteric conformation change in hexameric insulin, *Biopolym.: Biospectrosc. 58*, 249−260.
38. Smith, G. D., and Dodson, G. G. (1992) The structure of a rhombohedral R_6 insulin hexamer that binds phenol, *Biopolymers 32*, 1749−1756.
39. Turkenberg, M. G. W., Whittingham, J. L., Turkenberg, J. P., Dodson, G. G., Derewenda, U., Smith, G. D., Dodson, E. J., Derewenda, A. S., and Xiao, B. (1967) Insulin, monoclinic crystal form, Protein Data Bank entry 1ZNJ.

BI050392S